nature biomedical engineering

ARTICLES

https://doi.org/10.1038/s41551-019-0357-8

Adenine base editing in an adult mouse model of tyrosinaemia

Chun-Qing Song[1,14], Tingting Jiang[1,14], Michelle Richter[2,3,4], Luke H. Rhym[5,6], Luke W. Koblan[2,3,4], Maria Paz Zafra[7], Emma M. Schatoff[7,8], Jordan L. Doman[2,3,4], Yueying Cao[1], Lukas E. Dow[7], Lihua Julie Zhu[9,10,11], Daniel G Anderson[5,6], David R. Liu[2,3,4*], Hao Yin[12*] and Wen Xue[1,9,11,13*]

In contrast to traditional CRISPR–Cas9 homology-directed repair, base editing can correct point mutations without supplying a DNA-repair template. Here we show in a mouse model of tyrosinaemia that hydrodynamic tail-vein injection of plasmid DNA encoding the adenine base editor (ABE) and a single-guide RNA (sgRNA) can correct an A>G splice-site mutation. ABE treatment partially restored splicing, generated fumarylacetoacetate hydrolase (FAH)-positive hepatocytes in the liver, and rescued weight loss in mice. We also generated FAH$^+$ hepatocytes in the liver via lipid-nanoparticle-mediated delivery of a chemically modified sgRNA and an mRNA of a codon-optimized base editor that displayed higher base-editing efficiency than the standard ABEs. Our findings suggest that adenine base editing can be used for the correction of genetic diseases in adult animals.

Point mutations are a frequent cause of genetic diseases, with approximately 50% of disease-associated point mutations being G:C>A:T[1]. CRISPR genome editing, which consists of generating double-stranded DNA breaks followed by nonhomologous end-joining (NHEJ) or homology-directed repair (HDR), has been applied to many organisms[2,3]. However, major caveats of correcting point mutations through CRISPR genome editing include system efficiency, the introduction of double-stranded DNA breaks and the need to provide a DNA-repair template. A new generation of genome-editing tools, the base editing system, enables precise base changes[4,5], does not induce a high level of double-stranded DNA breaks and does not require HDR donors for gene repair[4,5].

To date, two classes of base editors have been developed[1,6]. Cytosine base editors, which include cytosine deaminases, Cas9 nickases and the uracil glycosylase inhibitor, introduce C•G to T•A base changes[6] and have been used to successfully introduce a stop codon or correct T•A to C•G mutations in prokaryotes, fungi, plants, insects, amphibians, fish and mammals[5,7–11]. ABEs comprise an evolved *Escherichia coli* TadA (*Ec*TadA*, a tRNA adenosine deaminase evolved to accept DNA substrate) and Cas9 nickase and mediate A•T to G•C substitutions[1]. Local delivery of ABEs by intramuscular injection of a trans-splicing adeno-associated virus was recently reported[12]; however, systemic delivery of ABEs for correction of liver disease in adult animals has not been investigated.

To explore the therapeutic potential of ABEs in the liver of adult animals, we chose a mouse model of hereditary tyrosinaemia type I (HTI), a fatal genetic disease. HTI is caused by loss of function of fumarylacetoacetate hydrolase (FAH), a key enzyme of the tyrosine catabolic pathway[13,14]. FAH deficiency leads to accumulation of toxic metabolic intermediates, causing apoptosis of mutant hepatocytes and severe liver damage. The *Fah$^{mut/mut}$* mouse model[14,15] has a homozygous G•C to A•T point mutation in the last nucleotide of exon 8, resulting in exon skipping and loss of FAH. 2-(2-nitro-4-trifluoromethylbenzoyl)-1,3-cyclohexanedione (NTBC)[14] is an inhibitor of the tyrosine catabolic pathway upstream of FAH. To be kept alive, *Fah$^{mut/mut}$* mice need to be treated with NTBC-supplemented water to prevent the build-up of toxins and liver damage[14].

We and others recently reported that CRISPR can correct this mutation in *Fah* through HDR[16–18] or allelic exchange[19]. Following correction by CRISPR, liver cells that express the FAH enzyme, through their selective advantage, expand and repopulate the liver[14]. Thus, this mouse model is particularly suitable for testing ABEs[13,15].

Results

Using adenine base editing to correct a *Fah* point mutation. The adenine base-editing window occupies positions ~4–9 with the first, 5′ nucleotide (nt) of the candidate sgRNA counted as position 1[1]. To edit the mutation in *Fah* using ABEs, we selected a previously validated *Fah* sgRNA[20] (Fig. 1a). The disease-associated point mutation is located at position 9 (A9). This sgRNA has the only sgRNA position that contains the necessary 'NGG' protospacer-adjacent motif and targets the mutation 'A' within the adenine base-editing window. Notably, ABE-mediated editing at position A6 will change a serine codon into alanine (S235A), but this editing will not restore splicing. Initially, we tested different doses of two ABE enzymes with different base-editing windows[1], ABE6.3 and ABE7.10, in *Fah* mutant mouse embryonic fibroblasts (MEFs). Consistent with the

[1]RNA Therapeutics Institute, University of Massachusetts Medical School, Worcester, MA, USA. [2]Department of Chemistry and Chemical Biology, Harvard University, Cambridge, MA, USA. [3]Howard Hughes Medical Institute, Harvard University, Cambridge, MA, USA. [4]Broad Institute of MIT and Harvard, Cambridge, MA, USA. [5]David H. Koch Institute for Integrative Cancer Research, Massachusetts Institute of Technology, Cambridge, MA, USA. [6]Department of Chemical Engineering, Massachusetts Institute of Technology, Cambridge, MA, USA. [7]Sandra and Edward Meyer Cancer Center, Department of Medicine, Weill Cornell Medicine, New York, NY, USA. [8]Weill Cornell/Rockefeller/Sloan Kettering Tri-I MD-PhD program, New York, NY, USA. [9]Department of Molecular, Cell and Cancer Biology, University of Massachusetts Medical School, Worcester, MA, USA. [10]Program in Bioinformatics and Integrative Biology, University of Massachusetts Medical School, Worcester, MA, USA. [11]Department of Molecular Medicine, University of Massachusetts Medical School, Worcester, MA, USA. [12]Medical Research Institute, Wuhan University, Wuhan, China. [13]Li Weibo Institute for Rare Diseases Research, University of Massachusetts Medical School, Worcester, MA, USA. [14]These authors contributed equally: Chun-Qing Song, Tingting Jiang. *e-mail: drliu@fas.harvard.edu; haoyin@whu.edu.cn; Wen.Xue@umassmed.edu

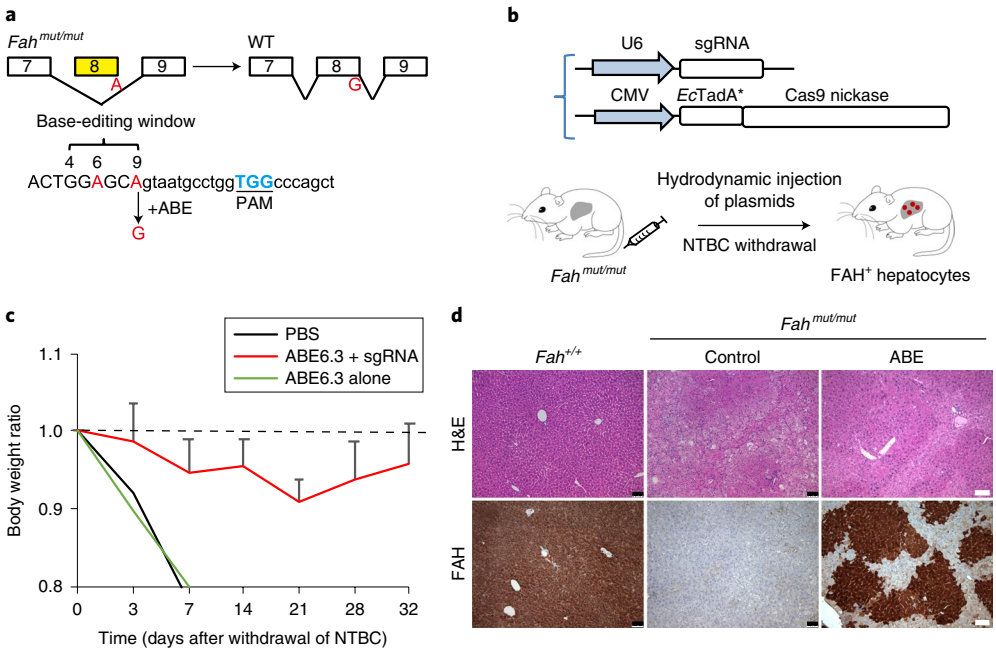

Fig. 1 | Adenine base editing rescues liver disease phenotype in a mouse model of tyrosinaemia. a, The G>A mutation (red) at the last nucleotide of exon 8 of the *Fah* gene of *Fah*$^{mut/mut}$ mice causes exon skipping. Exon sequences are shown in upper case. The G>A mutation is at position 9 of the sgRNA target. WT, wild-type allele. **b**, Hydrodynamic injection of ABE and sgRNA plasmids. **c**, Injection of ABE6.3 and sgRNA rescues body weight loss. Withdrawal of NTBC water is defined as day 0. Data are mean + s.d. ($n = 5$ mice). In the group treated with ABE6.3 and sgRNA, the final body weight is significantly different from the lowest weight ($P = 0.02$, one-tailed Student's *t*-test). **d**, ABE-treated mice show regions of FAH$^+$ hepatocytes ($n = 3$ mice, 32 days without NTBC). ABE, ABE plasmid + *Fah* sgRNA; H&E, haematoxylin and eosin. Scale bars, 75 μm.

literature[1], ABE6.3 resulted in the highest A>G base-editing efficiency at position A9 (6.9 ± 2.0%,2 μg ABE6.3, compared to an efficiency of 2.69 ± 1.14 for ABE7.10) (Supplementary Fig. 1) and editing efficiency was dependent of the concentration of the ABE enzyme. We therefore chose to test ABE6.3 in mice.

Adenine base editing generates FAH$^+$ hepatocytes in the liver of adult mice. To deliver ABEs to the liver of adult mice, we performed hydrodynamic tail-vein injection[21] with ABE6.3 and our validated *Fah* sgRNA plasmids (ABE hereafter, Fig. 1b). We removed NTBC-supplemented water 6 days after hydrodynamic injection to initiate HTI symptoms in *Fah*$^{mut/mut}$ mice. As shown in Fig. 1c, *Fah*$^{mut/mut}$ mice injected with control PBS or ABE6.3 alone rapidly lost 20% of their total body weight. By contrast, ABE6.3 and *Fah* sgRNA rescued weight loss in all five mice (Fig.1c).

To examine whether adenine base editing generates FAH$^+$ hepatocytes in vivo, we euthanized three of the five mice at day 32, collected the liver and stained liver sections with a FAH-specific antibody by immunohistochemistry (IHC). As shown in Fig. 1d and Supplementary Fig. 2, adenine base editor generated widespread patches of FAH$^+$ hepatocytes in the livers of *Fah*$^{mut/mut}$ mice owing to the expansion of corrected hepatocytes[14]. Concordantly, ABE-treated mice showed improved liver histology compared to the liver damage in control *Fah*$^{mut/mut}$ mice that did not receive NTBC water (Fig. 1d and Supplementary Fig. 3). Consistent with published literature[14,15], the rapid expansion of FAH$^+$ hepatocytes in the *Fah*$^{mut/mut}$ liver contributed to the rescue of weight loss in mice treated with ABEs[14]. These data indicate that adenine base editing rescues the disease phenotype caused by the *Fah* mutation in vivo.

To determine whether adenine base editing successfully corrects the HTI *Fah* splicing mutation in exon 8, we performed reverse transcription PCR (RT–PCR) in liver mRNA using primers that spanned exons 5 and 9. As shown in Fig. 2a, we found that the wild-type liver had a 405-bp PCR band that contained exon 8 and the *Fah*$^{mut/mut}$ liver had a 305-bp PCR band, which corresponds to the truncated form of *Fah* mRNA that lacks exon 8. In ABE-treated *Fah*$^{mut/mut}$ mice (after NTBC withdrawal and hepatocyte expansion), we observed both 305- and 405-bp PCR bands, indicating that exon 8 to exon 9 splicing was restored in a subset of hepatocytes. Sequencing of the 405-bp bands in ABE-treated mice confirmed the presence of the corrected 'G' at position A9 (Fig. 2b). These data indicate that in vivo delivery of ABEs corrects the G•C to T•A mutation in a subset of liver cells and generates functional exon 8-containing *Fah* mRNA.

Adenine base editing partially corrects the *Fah* mutation in the liver. To quantify the edited alleles after NTBC withdrawal, we amplified the *Fah* genomic region by PCR from liver DNA (using the same mice as in Fig. 1d) and performed amplicon deep sequencing. We observed that the A9 to G correction rate was 9.5 ± 4.0% ($n = 6$, Fig. 2c and Supplementary Table 1). Because many hepatocytes are 4*N* cells[20], it is possible that A9 in one allele was converted into G in the edited 4*N* hepatocytes.

Because position A6 of the *Fah* site is within the editing window of the ABE (Fig. 1a), we also evaluated the editing efficiency at this position. We detected 1.9 ± 0.9% A6 to G editing in the liver (Fig. 2c). Compared to in vitro editing in MEFs (Supplementary Fig. 1), the in vivo detection of relatively lower A6 to G editing is probably because of repopulation of A9-to-G-edited healthy cells in the liver rather than to an in vivo preference for A9 editing. The rate of both A6 to G and A9 to G editing (Fig. 2c) is low (around 0.1%). Editing position A6 to G will change a serine codon into alanine (S235A) in the FAH enzyme. Because S235 is near the active site of the FAH enzyme[22], the A6G/A9G allele may compromise enzyme activity and impede functional rescue of edited hepatocytes.

We also measured the rate of insertions and deletions (indels) by deep sequencing. The detected indel rate was very low (0.05% in

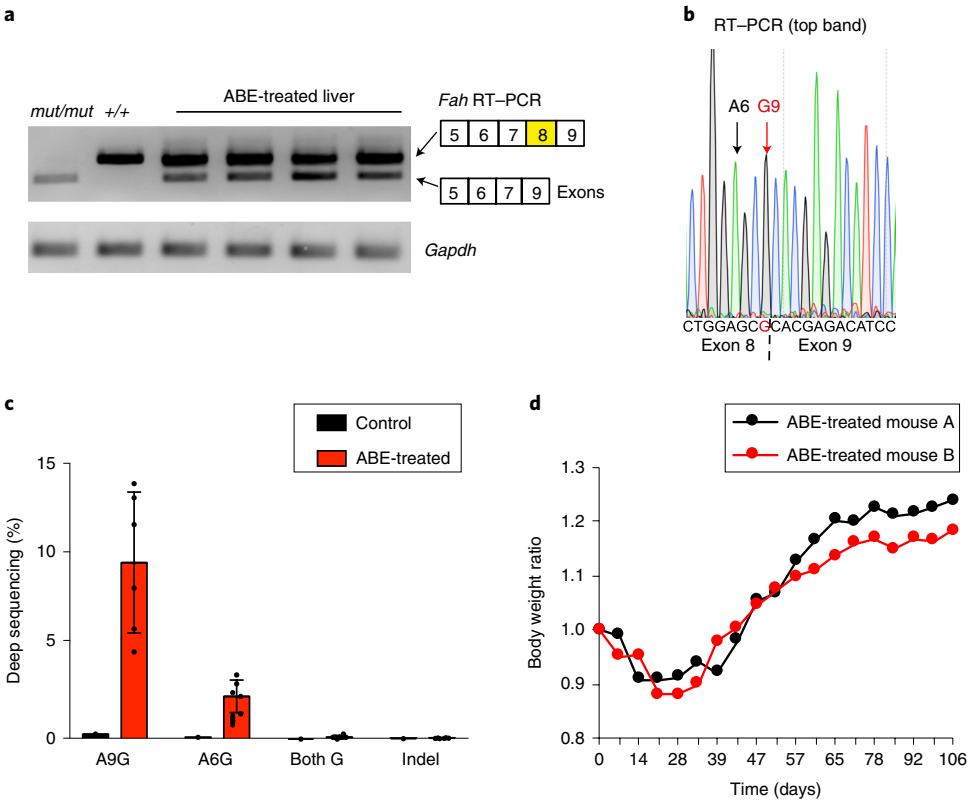

Fig. 2 | Adenine base editing partially corrects the *Fah* mutation in mouse liver. a, RT-PCR analysis of a representative ABE-treated mouse (four liver lobes) using primers that span exons 5 and 9. Wild-type *Fah* (+/+) amplicon is 405 bp and mutant *Fah* (which lacks exon 8) is 305 bp. *Gapdh* was used as control. Images of the uncropped gels are provided in Supplementary Fig. 10. **b**, Representative Sanger sequencing of the 405-bp RT-PCR bands. **c**, Deep sequencing of the *Fah* genomic region in liver DNA. Data are mean ± s.d. ($n = 6$ liver samples from two mice). **d**, Long-term survival of two ABE-treated mice (A and B) without NTBC.

ABE and 0.03% in control) even after expansion of the edited hepatocytes (Fig. 2c and Supplementary Table 2). These data suggest that ABE can directly correct the mutation in *Fah* without causing a high level of indel mutations. The two remaining ABE-treated mice were viable with a normal body weight at 106 days without NTBC treatment (Fig. 2d and Supplementary Fig. 4), demonstrating the long-term viability and functionality of ABE-treated hepatocytes.

Analysis of the off-target activity of ABE. To globally identify the off-target activity of ABE, we performed genome-wide Guide-seq[23] in vitro followed by in vivo deep sequencing at selected off-target sites in mouse livers. First, we evaluated off-target activity in vitro using mouse Hepa1-6 cells stably expressing Cas9 and transfected with sgFah and Guide-seq oligomers[16]. Using the standard Guide-seq protocol, we detected only the *Fah* target site and one off-target site (defined as Guide-seq off-target site 1, or GOT1) (Supplementary Data 1). These data suggest that the *Fah* sgRNA used in this study is not associated with a large number of strong off-target sites. Next, we performed targeted deep sequencing in vivo in both control and ABE-treated livers. We did not detect increased A•T to G•C editing at GOT1 in ABE-treated livers compared to controls ($n = 4$ mice, $P > 0.05$) (Supplementary Fig. 5).

To expand our analysis, we sequenced four predicted top-ranking off-target sites in ABE-treated livers ($n = 6$) and did not detect A•T to G•C editing above the background level in a control liver (all rates were less than 0.1%) (Supplementary Fig. 6). Because the overall on-target ABE efficiency in our *in vivo* study is relatively low, detecting off-target effects is difficult. Future work is needed to further study potential off-target editing of ABE[24,25].

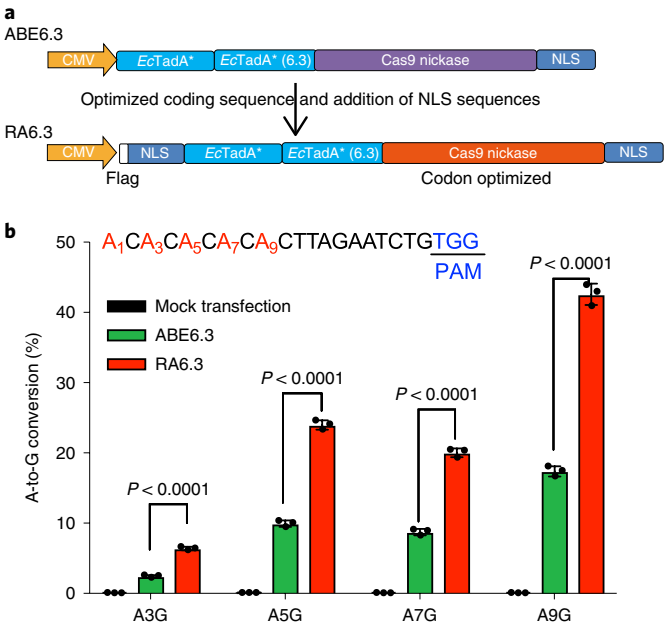

Fig. 3 | Optimizing the coding sequence of ABE6.3 and adding an N-terminal nuclear localization sequence improves base editing. a, Schematic representation of codon-optimized ABE6.3. NLS, nuclear localization sequence. **b**, Frequency of A-to-G editing in HEK293T cells 5 days after ABE and sgRNA transfection. Data are mean ± s.d. ($n = 3$ biologically independent samples). *P* values were determined by one-tailed Student's *t*-tests.

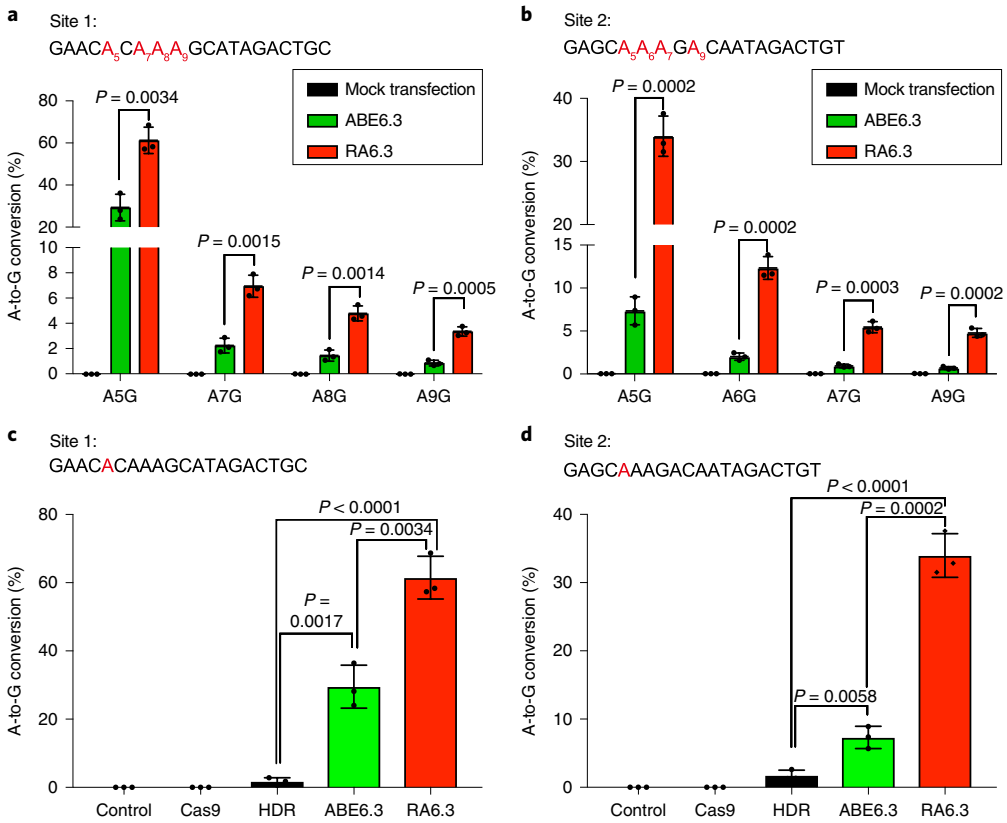

Fig. 4 | RA6.3 shows a higher editing efficiency compared to ABE6.3 and Cas9-mediated HDR at two genomic sites in HEK293T cells. a,**b**, Frequency of A-to-G editing at different positions at two genomic sites (sequences as indicated). The 'A's within the editing window are shown in red. **c**,**d**, Frequency of A-to-G conversion at a targeted A (in red) mediated by ABE6.3, RA6.3 or HDR at two genomic sites (sequences as indicated). Cas9 indicates the group transfected with Cas9 plasmid alone. Data are mean ± s.d. ($n = 3$ biologically independent samples). *P* values were determined by one-tailed Student's *t*-tests.

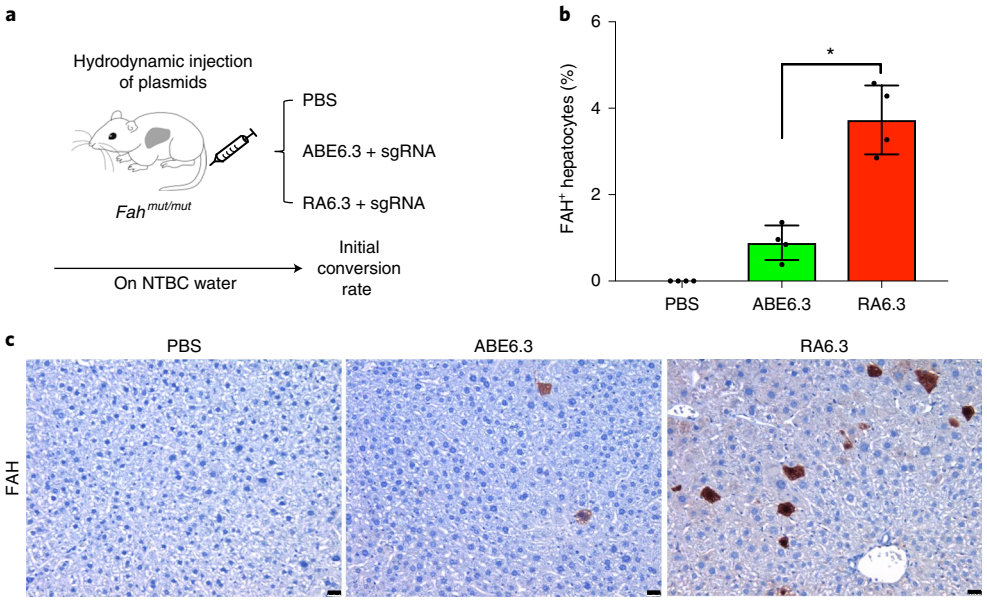

Fig. 5 | RA6.3 increases editing efficiency in vivo compared to ABE6.3. a, *Fah*$^{mut/mut}$ mice were injected with indicated plasmid combinations. To measure the initial A-to-G conversion rate, mice were kept on NTBC to prevent expansion of corrected cells. **b**, Quantification of FAH$^+$ hepatocytes by IHC at day 7. Data are mean ± s.d. ($n = 4$ mice per group). *$P = 0.0143$ by one-tailed Mann–Whitney *U*-test. **c**, Representative FAH IHC images. Scale bars, 25 μm.

A codon-optimized RA6.3 improves ABE activity. New reports have indicated that the efficiency of base editing can be improved with codon optimization of the Cas9 nickase and inclusion of an N-terminal nuclear localization sequence[26,27]. Optimized cytosine base editors and ABE7.10 have been reported[26,27]; however, optimization of ABE6.3 has not been performed. To test whether we could improve *Fah* base editing in our system, we cloned an optimized Cas9 nickase[26] into ABE6.3 (Fig. 3a) (called reassembled ABE6.3 or RA6.3). When transiently transfected in cells, our optimized base editor, RA6.3, showed substantially higher expression than ABE6.3 (Supplementary Fig. 7). To validate the efficiency of our optimized base editor, we transfected HEK293T cells with a selected sgRNA sequence with multiple 'A' sites[1] to evaluate A•T to G•C substitution by position (Fig. 3b). Deep sequencing showed an increase of base-editing efficiency at all adenine positions (including A9) with use of our codon-optimized ABE RA6.3 (Fig. 3b).

To further confirm that RA6.3 improves editing efficiency, we compared the A-to-G conversion efficiency of ABE6.3 and RA6.3 at two other genomic sites in HEK293T cells (Fig. 4a,b). Our optimized RA6.3 increased A-to-G conversion rate at all the editable 'A' sites within the editing window by an average of 2.1 ± 0.9-fold (site 1) and 4.8 ± 1.8-fold (site 2). Next, we compared the editing efficiency of HDR (100-nt single-stranded donor DNA)[1], ABE6.3 and RA6.3 at two genomic sites in HEK293T cells (Fig. 4c,d). Compared with HDR using short homologous arms (site 1:1.7 ± 1.1%; site 2: 1.8 ± 0.8%), ABE6.3 mediated substantially higher A•T to G•C conversion rates at the targeted sites (site 1: 30 ± 6.3%; site 2: 7.3 ± 1.6%), whereas RA6.3 further increased base-editing efficiency (site 1: 61 ± 6.3%; site 2: 34 ± 3.2%). These results confirm that the optimized ABE6.3 variant improves editing efficiency in cultured cells.

To compare RA6.3 and ABE6.3 in vivo, we measured the *Fah* editing efficiency following hydrodynamic injection of plasmids (Fig. 5a). IHC staining showed that RA6.3 generated more FAH$^+$ hepatocytes than ABE6.3 (Fig. 5b,c, $P < 0.05$). This result was confirmed by deep sequencing of the *Fah* target site (Supplementary Fig. 8a). In addition, RA6.3 increased base editing at a second mouse genomic site in vivo compared to ABE6.3 (Supplementary Fig. 8b). Our combined in vitro and in vivo results indicate that RA6.3 is a robust base editor in mammalian cells and in the mouse liver.

Lipid nanoparticle-mediated delivery of ABE mRNA and sgRNA in vivo. Finally, we used lipid nanoparticle (LNP)-mediated delivery[28] through tail-vein injection to deliver our optimized RA6.3 mRNA with chemically modified single-guide RNA to the liver of adult mice (Supplementary Fig. 9a). To measure initial ABE efficiency, we kept the mice on NTBC water after intravenous injection to prevent hepatocyte proliferation. As shown in Supplementary Fig. 9b, IHC images of the liver of *Fah*$^{mut/mut}$ mice injected with control PBS did not show any edited hepatocytes. By contrast, RA6.3 mRNA and *Fah* sgRNA showed 0.44% ± 0.28% edited hepatocytes (Supplementary Fig. 9c). The data suggest that non-viral delivery of ABEs is possible in the adult mouse liver and indicate the need to improve ABE mRNA stability and delivery vehicles.

Discussion

In summary, our results demonstrate that transient delivery of ABE6.3 and sgRNA by non-viral hydrodynamic injection is sufficient to generate FAH$^+$ hepatocytes and rescue the phenotypic weight loss of *Fah*-mutant mice. We codon-optimized ABE6.3 and showed that in vivo delivery of ABEs was able to correct the mutation in *Fah* in vivo without inducing high level of indels. The relatively low rate of indel formation is one notable advantage of ABE-mediated gene correction compared to Cas9-mediated HDR. Although we show phenotypic rescue in our *Fah*$^{mut/mut}$ mice, the in vivo ABE efficacy in our proof-of-concept study may not suffice to treat other genetic disorders that require higher levels of correction and that do not selectively proliferate corrected cells. Thus, further improvement of ABEs and delivery methods will continue to expand the utility of these tools.

As an initial delivery vehicle, our study also showed that non-viral LNP delivery of ABE mRNA and sgRNA generates FAH$^+$ hepatocytes in vivo, albeit with low efficiency. Because ABE mRNA is longer than Cas9 mRNA (5.2 kb compared to 4.1 kb, respectively), it is possible that the delivery or translation of ABE mRNA is less efficient than Cas9 mRNA. Methods to improve delivery and to enhance mRNA stability and/or translation will be required to broaden the therapeutic application of ABEs. This study demonstrates the potential application of adenine base editing to correct disease genes with G•C to T•A point mutations in adult mammalian models.

Methods

Construction of CRISPR vectors. The sgRNA vector (U6_sgRNA_EFS_GFP, Addgene 65656) expressing sgRNA[29] was digested with BsmBI. sgRNA oligomers were annealed, phosphorylated by T4 PNK and ligated with a linearized vector. RA6.3 vectors were cloned by Gibson assemble.

Mouse experiments. All mice study protocols were approved by the UMass IACUC. *Fah*$^{mut/mut}$ mice[14] were kept on 10 mg l^{-1} NTBC water. Mice with more than 20% weight loss were humanely euthanized according to guidelines. Vectors for hydrodynamic tail-vein injection were prepared using the EndoFreeMaxi kit (Qiagen). For hydrodynamic liver injection, plasmids suspended in 2 ml saline were injected via the tail vein in 5–7 s into 8–10-week-old *Fah*$^{mut/mut}$ mice. The plasmid doses were: Figs. 1, 2: 30 μg ABE plasmid and 60 μg sgFah plasmid; Fig. 5 and Supplementary Fig. 8a: 30 μg ABE plasmid (or 30 μg RA6.3) and 30 μg sgFah plasmid; Supplementary Fig. 8b: 30 μg ABE plasmid (or 30 μg RA6.3) and 15 μg sgAbc plasmid. The ABE RA6.3 mRNA was synthesized by TRILINK and the end-modified sgRNA was synthesized by Axolabs. The LNP formulation and treatment protocols were previously published[28]. In brief, 1 mg kg^{-1} LNP RA6.3 mRNA and 0.5 mg kg^{-1} LNP *Fah* sgRNA were injected in 8–10-week-old female *Fah*$^{mut/mut}$ mice via tail-vein injection. The mice were injected with 3–4 doses (every 3 days) and kept on NTBC water. Mice were euthanized 5 days after the last injection and organs were collected for analyses.

Immunohistochemistry. Mice were euthanized by carbon dioxide asphyxiation. Livers were fixed with 4% formalin, embedded in paraffin, sectioned at 5 μm and stained with haematoxylin and eosin for pathology. Liver sections were dewaxed, rehydrated and stained using standard IHC protocols[30]. The following antibody was used: anti-FAH (Abcam, 1:400). Representative images (of a total of more than 5 images) are shown.

Gene expression analysis and RT–PCR. RNA was purified using TRIzol (Invitrogen) and reverse-transcribed using a High-Capacity cDNA Reverse Transcription kit (Applied Biosystems). Full gel scans are shown in Supplementary Fig. 10.

Illumina sequencing. *Fah*$^{mut/mut}$ MEFs were transformed by retroviral WZL-HRas^{V12} and MSCV-shp53[31] to enhance transfection efficiency. ABE plasmids were electroporated into *Fah*$^{mut/mut}$ MEFs. The genomic region containing *Fah* was amplified using PCR. Deep-sequencing libraries were made from approximately 1–100 ng of the PCR products. Libraries were normalized to approximately equal molar ratio and sequenced on Illumina MiSeq machines (150-bp, paired-end reads). Reads were mapped to the PCR amplicons as references using bwa with custom scripts (available from the supplementary note of a previous study[1]). Data processing was performed according to standard Illumina sequencing analysis procedures.

Comparison of ABE6.3, RA6.3 and HDR. HEK293T cells were seeded at a confluence of 60%. After 24 h, cells were transfected with 1 μg Cas9 or base editors, 300 ng sgRNA expression plasmid, 6 μl Lipofectamine 3000 (Thermo Fisher Scientific) and for HDR assays, 0.7 μg single-stranded donor DNA template (100 nt, PAGE-purified from IDT)[1]. Genomic DNA was collected 72 h after transcription using quickextract buffer (Epicentre). Deep sequencing was performed to measure A to G conversion. Single-stranded 100-mer oligonucleotide donor templates and primers are listed in Supplementary Tables 3 and 4.

Guide-seq. Deep-sequencing data from the Guide-seq experiment were analysed using the GUIDEseq v.1.10.0 Bioconductor package[32] after barcode deconvolution, adaptor removal and alignment to the mouse genome (mm10). The default settings for *Sp*Cas9 are used except that min.reads is set to 2 and min.peak.score.1strandOnly is set to 2 as described previously[33].

Reporting Summary. Further information on research design is available in the Nature Research Reporting Summary linked to this article.

Data availability

The authors declare that all data supporting the findings of this study are available within the paper and its Supplementary Information. The deep-sequencing data are available from the Sequence Read Archive (SRA) under accession number PRJNA513076 and PRJNA513291.

Received: 13 August 2018; Accepted: 16 January 2019;
Published online: 25 February 2019

References

1. Gaudelli, N. M. et al. Programmable base editing of A•T to G•C in genomic DNA without DNA cleavage. *Nature* **551**, 464–471 (2017).
2. Cong, L. et al. Multiplex genome engineering using CRISPR/Cas systems. *Science* **339**, 819–823 (2013).
3. Mali, P. et al. RNA-guided human genome engineering via Cas9. *Science* **339**, 823–826 (2013).
4. Hess, G. T., Tycko, J., Yao, D. & Bassik, M. C. Methods and applications of CRISPR-mediated base editing in eukaryotic genomes. *Mol. Cell* **68**, 26–43 (2017).
5. Rees, H. A. & Liu, D. R. Base editing: precision chemistry on the genome and transcriptome of living cells. *Nat. Rev. Genet.***19**, 770–788 (2018).
6. Komor, A. C., Kim, Y. B., Packer, M. S., Zuris, J. A. & Liu, D. R. Programmable editing of a target base in genomic DNA without double-stranded DNA cleavage. *Nature* **533**, 420–424 (2016).
7. Chadwick, A. C., Wang, X. & Musunuru, K. In vivo base editing of PCSK9 (proprotein convertase subtilisin/kexin type 9) as a therapeutic alternative to genome editing. *Arterioscler. Thromb. Vasc. Biol.* **37**, 1741–1747 (2017).
8. Kim, K. et al. Highly efficient RNA-guided base editing in mouse embryos. *Nat. Biotechnol.* **35**, 435–437 (2017).
9. Zong, Y. et al. Precise base editing in rice, wheat and maize with a Cas9–cytidine deaminase fusion. *Nat. Biotechnol.* **35**, 438–440 (2017).
10. Rossidis, A. C. et al. In utero CRISPR-mediated therapeutic editing of metabolic genes. *Nat. Med.* **24**, 1513–1518 (2018).
11. Villiger, L. et al. Treatment of a metabolic liver disease by in vivo genome base editing in adult mice. *Nat. Med.* **24**, 1519–1525 (2018).
12. Ryu, S. M. et al. Adenine base editing in mouse embryos and an adult mouse model of Duchenne muscular dystrophy. *Nat. Biotechnol.* **36**, 536–539 (2017).
13. Azuma, H. et al. Robust expansion of human hepatocytes in *Fah*$^{-/-}$/*Rag2*$^{-/-}$/*Il2rg*$^{-/-}$ mice. *Nat. Biotechnol.* **25**, 903–910 (2007).
14. Paulk, N. K. et al. Adeno-associated virus gene repair corrects a mouse model of hereditary tyrosinemia in vivo. *Hepatology* **51**, 1200–1208 (2010).
15. Aponte, J. L. et al. Point mutations in the murine fumarylacetoacetate hydrolase gene: animal models for the human genetic disorder hereditary tyrosinemia type 1. *Proc. Natl Acad. Sci. USA* **98**, 641–645 (2001).
16. Yin, H. et al. Therapeutic genome editing by combined viral and non-viral delivery of CRISPR system components in vivo. *Nat. Biotechnol.* **34**, 328–333 (2016).
17. Song, C. Q. & Xue, W. CRISPR–Cas-related technologies in basic and translational liver research. *Nat. Rev. Gastroenterol. Hepatol.* **15**, 251–252 (2018).
18. Shao, Y. et al. Cas9-nickase-mediated genome editing corrects hereditary tyrosinemia in rats. *J. Biol. Chem.* **293**, 6883–6892 (2018).
19. Wang, D. et al. Cas9-mediated allelic exchange repairs compound heterozygous recessive mutations in mice. *Nat. Biotechnol.* **36**, 839–842 (2018).
20. Yin, H. et al. Genome editing with Cas9 in adult mice corrects a disease mutation and phenotype. *Nat. Biotechnol.* **32**, 551–553 (2014).
21. Liu, F., Song, Y. & Liu, D. Hydrodynamics-based transfection in animals by systemic administration of plasmid DNA. *Gene Ther.* **6**, 1258–1266 (1999).
22. Bateman, R. L. et al. Mechanistic inferences from the crystal structure of fumarylacetoacetate hydrolase with a bound phosphorus-based inhibitor. *J. Biol. Chem.* **276**, 15284–15291 (2001).
23. Tsai, S. Q. et al. GUIDE-seq enables genome-wide profiling of off-target cleavage by CRISPR–Cas nucleases. *Nat. Biotechnol.* **33**, 187–197 (2015).
24. Lee, H. K. et al. Targeting fidelity of adenine and cytosine base editors in mouse embryos. *Nat. Commun.* **9**, 4804 (2018).
25. Liang, P. et al. Genome-wide profiling of adenine base editor specificity by EndoV-seq. *Nat. Commun.* **10**, 67 (2019).
26. Zafra, M. P. et al. Optimized base editors enable efficient editing in cells, organoids and mice. *Nat. Biotechnol.* **36**, 888–893 (2018).
27. Koblan, L. W. et al. Improving cytidine and adenine base editors by expression optimization and ancestral reconstruction. *Nat. Biotechnol.* **36**, 843–846 (2018).
28. Yin, H. et al. Structure-guided chemical modification of guide RNA enables potent non-viral in vivo genome editing. *Nat. Biotechnol.* **35**, 1179–1187 (2017).
29. Hsu, P. D. et al. DNA targeting specificity of RNA-guided Cas9 nucleases. *Nat. Biotechnol.* **31**, 827–832 (2013).
30. Xue, W. et al. Response and resistance to NF-kB inhibitors in mouse models of lung adenocarcinoma. *Cancer Discov.* **1**, 236–247 (2011).
31. Xue, W. et al. Senescence and tumour clearance is triggered by p53 restoration in murine liver carcinomas. *Nature* **445**, 656–660 (2007).
32. Zhu, L. J. et al. GUIDEseq: a Bioconductor package to analyze GUIDE-seq datasets for CRISPR–Cas nucleases. *BMC Genomics* **18**, 379 (2017).
33. Yin, H. et al. Partial DNA-guided Cas9 enables genome editing with reduced off-target activity. *Nat. Chem. Biol.* **14**, 311–316 (2018).

Acknowledgements

We thank C. Mello, P. Zamore, S. Wolfe and E. Sontheimer for discussions; J. Smith for editing the manuscript; M. Grompe (Oregon Health and Science University) for providing the *Fah* mice; Y. Liu and E. Kittler of the UMass Morphology and Deep Sequencing Cores for support. W.X. was supported by grants from the National Institutes of Health ((NIH) DP2HL137167, P01HL131471 and UG3HL147367), American Cancer Society (129056-RSG-16-093), the Lung Cancer Research Foundation, Hyundai Hope on Wheels, UMass CCTS and ALS Association. This work was supported by DARPA HR0011-17-2-0049; US NIH RM1 HG009490, R01 EB022376, U01 AI142756 and R35 GM118062; and HHMI (to D.R.L.), and R01 CA195787; K22 CA181280 (to L.E.D.). This work was supported in part by the Marble Center for Cancer Nanomedicine and a Cancer Center Support (core) grant P30-CA14051 from the National Cancer Institute. M.R. was supported by the HHMI Hanna H. Gray Fellowship. L.W.K. is an NSF Graduate Research Fellow and was supported NIH Training Grant T32 GM095450. H.Y. was supported by the National Natural Science Foundation of China 31871345, the Young Thousand Talented Program from Wuhan University and startup funding from Wuhan University.

Author contributions

C.Q.S., T.J., M.R., D.R.L., H.Y. and W.X. designed the study. C.Q.S., T.J., M.R., L.H.R., L.W.K., M.P.Z., E.M.S., J.L.D., Y.C., L.J.Z., L.E.D. and D.G.A. performed experiments and analysed data. C.Q.S., T.J., H.Y. and W.X. wrote the manuscript with comments from all authors.

Competing interests

D.R.L. is a consultant and co-founder of Editas Medicine, Pairwise Plants and Beam Therapeutics, which are companies that use genome editing. The other authors declare no competing interests.

Additional information

Supplementary information is available for this paper at https://doi.org/10.1038/s41551-019-0357-8.

Reprints and permissions information is available at www.nature.com/reprints.

Correspondence and requests for materials should be addressed to D.R.L., H.Y. or W.X.

Publisher's note: Springer Nature remains neutral with regard to jurisdictional claims in published maps and institutional affiliations.

nature research

Corresponding author(s): David Liu, Hao Yin and Wen Xue

Reporting Summary

Nature Research wishes to improve the reproducibility of the work that we publish. This form provides structure for consistency and transparency in reporting. For further information on Nature Research policies, see Authors & Referees and the Editorial Policy Checklist.

Statistical parameters

When statistical analyses are reported, confirm that the following items are present in the relevant location (e.g. figure legend, table legend, main text, or Methods section).

n/a	Confirmed	
☐	☒	The exact sample size (*n*) for each experimental group/condition, given as a discrete number and unit of measurement
☐	☒	An indication of whether measurements were taken from distinct samples or whether the same sample was measured repeatedly
☐	☒	The statistical test(s) used AND whether they are one- or two-sided *Only common tests should be described solely by name; describe more complex techniques in the Methods section.*
☒	☐	A description of all covariates tested
☒	☐	A description of any assumptions or corrections, such as tests of normality and adjustment for multiple comparisons
☒	☐	A full description of the statistics including central tendency (e.g. means) or other basic estimates (e.g. regression coefficient) AND variation (e.g. standard deviation) or associated estimates of uncertainty (e.g. confidence intervals)
☒	☐	For null hypothesis testing, the test statistic (e.g. *F*, *t*, *r*) with confidence intervals, effect sizes, degrees of freedom and *P* value noted *Give P values as exact values whenever suitable.*
☒	☐	For Bayesian analysis, information on the choice of priors and Markov chain Monte Carlo settings
☒	☐	For hierarchical and complex designs, identification of the appropriate level for tests and full reporting of outcomes
☒	☐	Estimates of effect sizes (e.g. Cohen's *d*, Pearson's *r*), indicating how they were calculated
☐	☒	Clearly defined error bars *State explicitly what error bars represent (e.g. SD, SE, CI)*

Our web collection on statistics for biologists may be useful.

Software and code

Policy information about availability of computer code

Data collection	MiSeq (Illumina)
Data analysis	Reads were mapped to the PCR amplicons as references using bwa with custom scripts (available in Supplementary Note 1 of ref. 1 in the paper).

For manuscripts utilizing custom algorithms or software that are central to the research but not yet described in published literature, software must be made available to editors/reviewers upon request. We strongly encourage code deposition in a community repository (e.g. GitHub). See the Nature Research guidelines for submitting code & software for further information.

Data

Policy information about availability of data

All manuscripts must include a data availability statement. This statement should provide the following information, where applicable:

- Accession codes, unique identifiers, or web links for publicly available datasets
- A list of figures that have associated raw data
- A description of any restrictions on data availability

The authors declare that all data supporting the findings of this study are available within the paper and its Supplementary Information. The deep-sequencing data is available at the Sequence Read Archive under the accession code PRJNA513076.

Field-specific reporting

Please select the best fit for your research. If you are not sure, read the appropriate sections before making your selection.

☒ Life sciences ☐ Behavioural & social sciences ☐ Ecological, evolutionary & environmental sciences

For a reference copy of the document with all sections, see nature.com/authors/policies/ReportingSummary-flat.pdf

Life sciences study design

All studies must disclose on these points even when the disclosure is negative.

Sample size	Experiments were done in biological triplicate in culture cells, n=3 on different days. In previous studies we determined this sample size to be sufficient to ensure reproducibility. For animal experiments, we described the size in the appropriate figure legends.
Data exclusions	No data were excluded.
Replication	All attempts at replication were successful, and standard deviations were in the expected ranges.
Randomization	The same cell passages were used for the biological replicates, and the results were confirmed by different cells passages.
Blinding	Blinding was not relevant.

Reporting for specific materials, systems and methods

Materials & experimental systems

n/a	Involved in the study
☒	☐ Unique biological materials
☐	☒ Antibodies
☐	☒ Eukaryotic cell lines
☒	☐ Palaeontology
☐	☒ Animals and other organisms
☒	☐ Human research participants

Methods

n/a	Involved in the study
☒	☐ ChIP-seq
☒	☐ Flow cytometry
☒	☐ MRI-based neuroimaging

Antibodies

Antibodies used	Anti-Fumarylacetoacetate hydrolase antibody (ab83770)
Validation	Rabbit polyclonal to Fumarylacetoacetate hydrolase, IHC 1:400

Eukaryotic cell lines

Policy information about cell lines

Cell line source(s)	HEK293T (ATTC) and Fah-mutant mouse embryonic fibroblasts.
Authentication	HEK293T (ATCC) cells were authenticated by the supplier. Fah-mutant MEF cells were separated from the Fah-mutant mice.
Mycoplasma contamination	The cell lines were not tested for mycoplasma contamination.
Commonly misidentified lines (See ICLAC register)	No commonly misidentified cell lines were used.

Animals and other organisms

Policy information about studies involving animals; ARRIVE guidelines recommended for reporting animal research

Laboratory animals	8–10-week-old female Fah mut/mut mice as a mouse model of tyrosinemia.

Wild animals	The study did not involve wide animals.
Field-collected samples	The study did not involve samples collected from the field.